# High Spin Effect on the Dynamics of a High $\ell/d$ Finned Projectile from Free-Flight Tests

Alain D. Dupuis*
*Defence Research Establishment Valcartier, Courcelette, Quebec, Canada*

**Free-flight data from tests of a 27 $\ell/d$ finned projectile over a Mach number range of 1.5 to 4 have been reduced to aerodynamic coefficients. Six model configurations varying in planform areas and tab angles were investigated. A summary of the aerodynamic data from these tests at low and high spin rates up to 3500 rad/s is given. Some aerodynamic coefficients exhibited a strong dependency on spin, and this is also discussed.**

## Nomenclature

| | |
|---|---|
| $C_x, C_N$ | = axial and normal force coefficients, respectively |
| $C_{\ell_p}$ | = roll damping coefficient |
| $C_{\ell_\delta}$ | = roll moment coefficient due to fin cant |
| $C_m, C_{n_{p\alpha}}$ | = pitching and Magnus moment coefficients, respectively |
| $C_{m_q}$ | = pitch damping coefficient |
| CG | = center of gravity |
| $d$ | = reference diameter |
| $I_x, I_y$ | = moments of inertia |
| $\ell$ | = model length |
| $M$ | = Mach number |
| $p$ | = spin rate |
| $p_\infty$ | = steady spin rate |
| PE$x$, PE$y$, $z$ | = probable error in range, swerve |
| PE$\theta$, $\psi$, PE$\phi$ | = pitch and yaw, and roll, respectively |
| $V$ | = velocity |
| $\alpha$ | = total angle of attack |
| $\alpha$ max | = maximum angle of attack |
| $\omega$ | = resonant frequency |

*Subscripts*

| | |
|---|---|
| p | = derivative with respect to $pd/2V$ |
| $\alpha$ | = derivative with respect to $\sin\alpha$ |

## Introduction

THIS establishment is currently engaged in research on high $\ell/d$ kinetic energy penetrators for 70-mm air-launched rocket application. One of the objectives of the program is to enlarge the free-flight aerodynamic data base of high $\ell/d$ finned projectiles. One configuration consisted of a 27 $\ell/d$ three-finned projectile that was tested at the Eglin Aeroballistic Research Facility under a joint U.S./Canadian project arrangement.

Some aerodynamic coefficients, especially the pitching moment coefficient slope, exhibited a strong dependence on spin in the low supersonic region, and this effect decreased as the Mach number increased. Various aspects that would cause this to occur have been studied, and the most plausible explanation is a static pitching moment coefficient slope linearly dependent on spin, that is, an in-plane Magnus effect.

Received June 3, 1987; presented as Paper 87-2430 at the AIAA Atmospheric Flight Mechanics Conference, Monterey, CA, Aug. 17-19, 1987; revision received Oct. 19, 1987. 

*Defense Scientist, Armaments Division.

## Facility Description

The free-flight tests were conducted in the Aeroballistics Research Facility (ARF),[1] which is part of the Ballistics Branch, U.S. Air Force Armament Laboratory, Eglin Air Force Base, Florida. This facility is an enclosed concrete structure used to examine the exterior ballistics of various free-flight configurations. The facility contains a gun room, control room, model measurements room, blast chamber, and the instrumented range.

The 207-m instrumented length of the range has a 3.6-m square cross section for the first 69-m and a 4.88-m square cross section for the remaining length. The range has 131 locations available as instrumentation sites at 1.52-m intervals, and currently 50 of the sites are used to house fully instrumented orthogonal shadowgraph stations. These stations yield photographs of the shadow of the projectile as it flies down the range. The maximum shadowgraph window, an imaginary circle in which a projectile in flight will cast a shadow on both reflective screens, is 2.13 m in diameter. A laser-lighted photographic station is located in the up-range end of the instrumented range. This photographic station yields four orthogonal photographs, permitting a complete 360-deg view of the projectile as it passes the station. Also, a direct shadowgraph station, consisting of a spark gap and film holder, is located near the start of the range. Since the film is illuminated directly by the spark as the model passes the station, high-quality flow photographs are obtained. The nominal operating conditions of the range are 22°C at standard atmospheric pressure.

## Models and Test Conditions

Six model configurations were investigated during the test program. The basic configuration consisted of a 15-deg nose cone on a cylindrical body, with a 6-deg boattail and two fin lengths, as shown in Fig. 1. The $\ell/d$ of the models was approximately 27. The longer-fin configuration had 25% more planform area than the shorter one. Both configurations were tested with nominal tab angles of 0, 2, and 4 deg on each fin, so that the nonzero angles would produce clockwise spin when viewed from the rear. The models were modified by the addition of a pin on one of the fins in order to measure the projectile's roll orientation (Fig. 2). The nominal diameter of the models was 6.35 mm, and they were made of steel.

All of the models were launched from a 30-mm smoothbore gun at atmospheric pressure conditions. Three types of sabots were initially developed, but a three-piece pusher type was chosen, and it functioned well throughout the velocity range of interest (550–1500 m/s). This design produced good separation at launch (Fig. 3), with the one disadvantage that the pusher followed the model through the instrumented range.

Usable data were obtained on 33 flights, which included 11 short-fin and 22 long-fin models. The average physical proper-

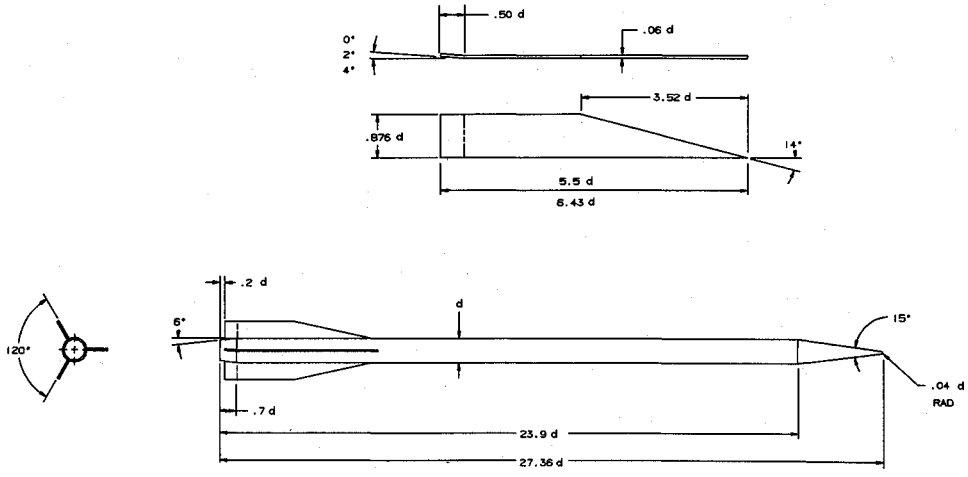


Fig. 1 Model configuration.

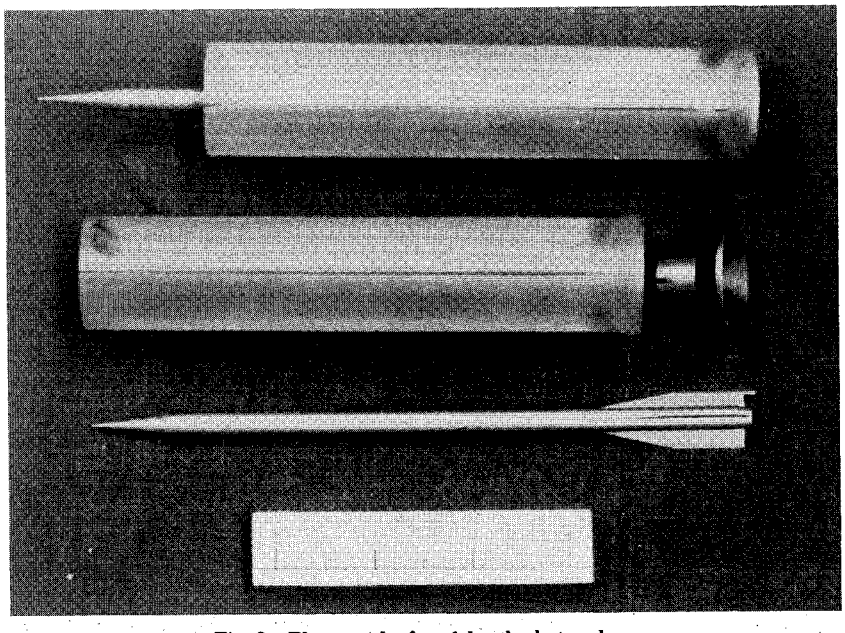

Fig. 2 Photograph of model and sabot package.

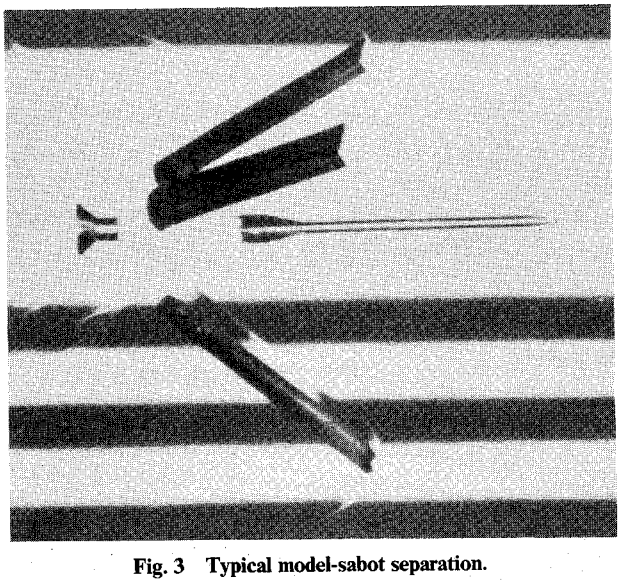

Fig. 3 Typical model-sabot separation.

ties of the models are listed in Table 1. Because the long-fin model covered the Mach number range of interest, only these results will be presented, and comments on the short-fin model will be made where appropriate.

Table 1 Average physical properties of models

| | Long fin | Short fin |
|---|---|---|
| Mass, gm | 40.60 | 40.24 |
| $I_x$, gm-cm$^2$ | 2.500 | 2.441 |
| $I_y$, gm-cm$^2$ | 897.2 | 887.8 |
| CG, % $\ell$ from nose | 55.15 | 54.89 |
| $d$, cm | 0.6343 | 0.6340 |
| $\ell$, cm | 17.375 | 17.374 |

## Free-Flight Data Reduction

Extraction of the aerodynamic coefficients and derivatives is the primary goal in analyzing the trajectories measured in the ARF. This is done by means of the Aeroballistics Research Facility Data Analysis System (ARFDAS)[2] shown in Fig. 4. ARFDAS incorporates a standard linear theory analysis and a six-degree-of-freedom (6-DOF) numerical integration technique. The 6-DOF routine incorporates the maximum likelihood method (MLM) to match the theoretical trajectory to the experimentally measured trajectory. The MLM is an iterative procedure that adjusts the aerodynamic coefficients to maximize a likelihood function. The application of this likelihood function eliminates the inherent assumption in least-squares theory that the magnitude of the measurement noise must be consistent between dynamic parameters (irrespective

of units). In general, the aerodynamic coefficients are nonlinear functions of angle of attack, Mach number, and roll angle.

ARFDAS represents a complete ballistic range data reduction system capable of analyzing both symmetric and unsymmetric models. The essential steps of the data reduction system are to 1) assemble the basic dynamic range data (time, position, angles), physical properties, and atmospheric conditions, 2) perform linear theory analysis, and 3) perform 6-DOF analysis.

These three steps have been integrated into ARFDAS to provide the test engineer with a convenient and efficient means of interaction. At each step in the analysis, permanent records for each shot are maintained so that subsequent analyses with data modifications are much faster.

The 6-DOF data reduction system can also simultaneously fit multiple data sets (up to five) to a common set of aerodynamics. Using this multiple-fit approach, a more complete range of angle of attack and roll orientation combinations is available for analysis than would be available from a single flight. This procedure increases the accuracy of the determined aerodynamics over the entire range of angle of attack and roll combinations.

The aerodynamic data presented in this paper were obtained using the fixed-plane 6-DOF analysis (MLMFXPL) with the single- and multiple-fit data correlation techniques. The equations of motion have been derived in a fixed-plane coordinate system, with Coriolis effects included. The formal derivation of the fixed-plane model is given in Ref. 2.

## Results and Discussion

The tab angles of the fins were measured at the tip and root of each fin, and an average of the three fins was taken. These average tab angles are given in Table 2 only for models that had tab angles and does not include the cant of the fin. The accuracy of these angles is approximately $\pm 0.5$ deg. The tab angles vary appreciably from the nominal values (2, 4 deg), and this is due mainly to manufacturing problems. Some tab angles were as high as 6 deg. The steady spin rate measured from the free-flight data in the ARF is included in Table 2 and is also given in nondimensional form ($pd/2V$) and as a function of the resonant frequency $\omega$. At the higher Mach numbers, it was not possible to obtain accurate roll data since there was difficulty in distinguishing the roll pin when reading the films. Therefore, it was not possible to solve for the roll-dependent terms in these cases. The range of spin was 0.6–18 times the resonant frequency, with at least one model just at the resonant frequency. The total angle of attack at launch was generally small, and there was difficulty reducing for $C_{N_\alpha}$, $C_{m_q}$, and $C_{n_{p\alpha}}$ in single fits.

**Table 2 Test conditions**

| Shot no. | Tab angle, deg | Mach no. | $\alpha$ max, deg | $p_\infty$, rad/s | $pd/2V$ | $p/\omega$ |
|---|---|---|---|---|---|---|
| 62 | 2.79 | 1.576 | 1.3 | 2158 | 0.01264 | 12.5 |
| 65 | 3.15 | 1.646 | 1.5 | 1662 | 0.00932 | 9.3 |
| 67 | 5.41 | 1.682 | 1.4 | 2768 | 0.01519 | 13.0 |
| 66 | 5.28 | 1.697 | 1.8 | 3531 | 0.01920 | 17.8 |
| 54 | 2.21 | 2.057 | 1.8 | 1532 | 0.00687 | 6.6 |
| 44 | 0.0 | 2.075 | 3.6 | 149 | 0.00066 | 0.63 |
| 57 | 4.98 | 2.159 | 3.2 | 3099 | 0.01325 | 12.1 |
| 47 | 0.0 | 2.194 | 1.2 | −230 | −0.00097 | 0.98 |
| 60 | 0.0 | 2.201 | 1.0 | 151 | 0.00063 | 0.63 |
| 52 | 5.98 | 2.785 | 4.0 | 2537 | 0.00841 | 8.3 |
| 45 | 0.0 | 2.812 | 1.9 | −160 | −0.00053 | 0.54 |
| 80 | 2.70 | 2.834 | 1.3 | 1703 | 0.00555 | 5.49 |
| 46 | 2.72 | 2.842 | 2.0 | 1571 | 0.00511 | 5.07 |
| 81 | 5.39 | 2.854 | 2.8 | 2447 | 0.00791 | 7.97 |
| 48 | 0.0 | 2.868 | 5.8 | −128 | −0.00041 | 0.42 |
| 82 | 5.60 | 3.187 | 1.6 | 1794 | 0.00520 | 5.43 |
| 74 | — | 3.602 | 3.0 | — | — | — |
| 72 | 0.0 | 3.632 | 3.0 | 442 | 0.00112 | 1.16 |
| 75 | — | 3.633 | 3.6 | — | — | — |
| 73 | — | 3.673 | 3.4 | — | — | — |
| 77 | — | 4.121 | 5.3 | — | — | — |
| 78 | — | 4.125 | 6.6 | — | — | — |

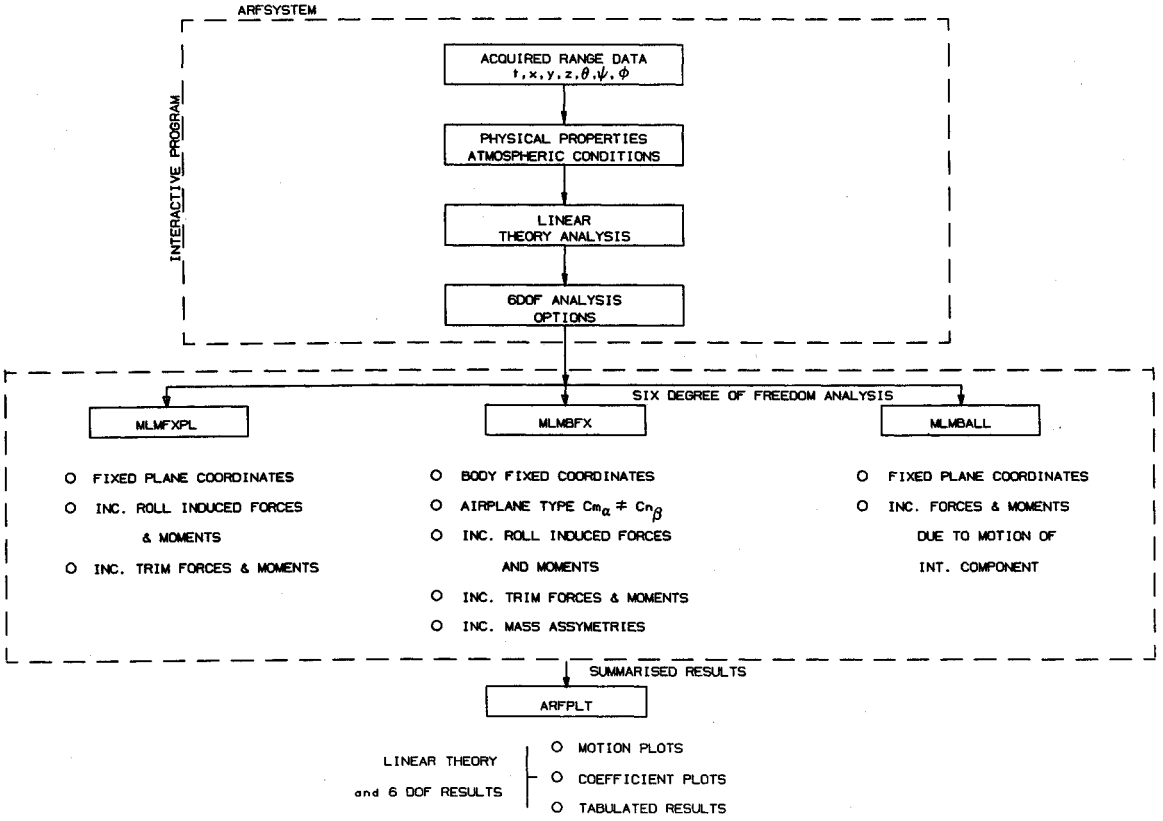


**Fig. 4 Aeroballistic research facility data analysis system.**

The 6-DOF single-fit results for $C_{m_\alpha}$, $C_{\ell_p}$, $C_{\ell_\delta}$, and $C_x$ are shown in Fig. 5. The moment reference of $C_{m_\alpha}$ is 55% from the nose. All of the coefficients show some scatter at a given Mach number and especially in the Mach number range 1.5–3.0. For example, there is a large scatter in $C_{m_\alpha}$ at $M \simeq 1.6$, 2.2, and 2.8, and the amount of scatter decreases as the Mach number increases. This scatter is also evident in $C_{\ell_p}$ and $C_{\ell_\delta}$. The data analysis system solves for a combined $C_{\ell_\delta}\delta$, which was very well determined. To obtain $C_{\ell_\delta}$, the above term is divided by the measured tab angle. Therefore, some of the scatter in $C_{\ell_\delta}$ is due to errors in measuring the tab angle. It was also assumed that the contribution of the whole fin to $C_{\ell_\delta}$ was negligible. The probable errors of fit are given in Table 3 and are consistent with the linear theory results. This kind of scatter at the same Mach number was not expected because the basic coefficients are the easiest ones to reduce.

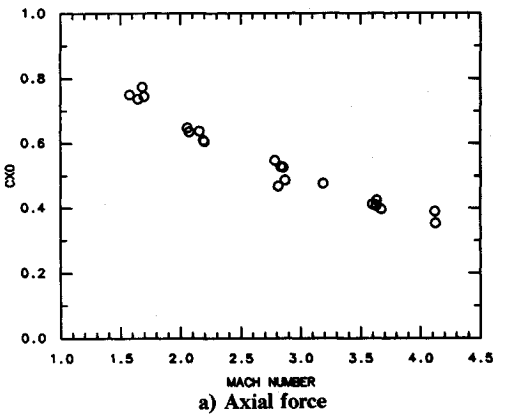

a) Axial force

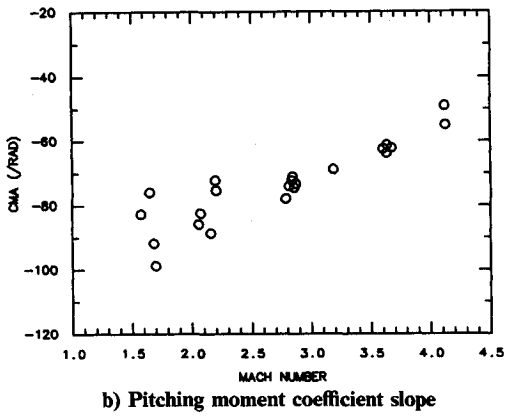

b) Pitching moment coefficient slope

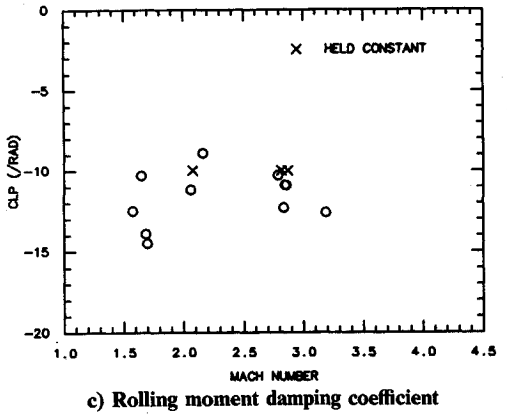

c) Rolling moment damping coefficient

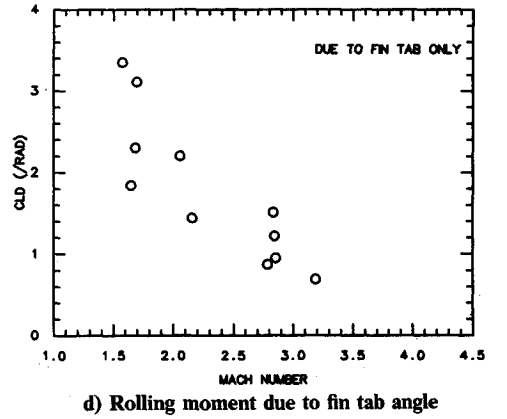

d) Rolling moment due to fin tab angle

**Fig. 5 Aerodynamic coefficients vs Mach number.**

Several aspects that could cause $C_{m_\alpha}$ and the other coefficients to vary at the same Mach number were investigated. The most obvious possible cause is damage to the projectile and especially to the fins at launch. All of the photographs of the models taken at Eglin, imprints on yaw cards during sabot development, and ballistic-synchro pictures show no damage to the fins. There is high confidence that the models were not damaged in the Mach number range 1.5–4.0. At the high supersonic numbers (Mach 4.0–4.5), the angle of attack was increasing on some shots as the model was going down range. Some models did go unstable in the Eglin trials and during sabot development at approximately Mach 4.5.

Bending of a projectile in flight can be caused when a projectile spins at a critical spin rate that is related to the frequency of the first longitudinal bending mode.[3,4] The extent of projectile bending at the critical spin rate depends on the associated mass asymmetry of the projectile. The free-free longitudinal bending frequency of the models is approximately 6211 rad/s, which is well above the spin rates that were achieved. Therefore, the possibility of being at the critical spin rate was ruled out as a possible cause for the scatter in the results.

Tables 2 and 3 indicate that the coefficients vary as the steady spin rate changes. This is most evident for $C_{m_\alpha}$ for the group at Mach 1.6 and 2.1; $C_{m_\alpha}$ increases in magnitude (i.e., is more stable) as the steady spin rate increases. A variation with spin rate is also evident for $C_{\ell_p}$ and $C_{\ell_\delta}$ at Mach 1.65. This spin dependence diminishes as the Mach number increases and is absent at the high Mach numbers.

Corrected for Mach number, $C_{m_\alpha}$ is plotted vs the absolute value of the nondimensional steady spin rate $pd/2V$ in Fig. 6 at Mach 1.65 and 2.1. The absolute value for the spin rate was

**Table 3 Aerodynamic results (single fits)**

| Shot no. | $-C_{m_\alpha}$ | $-C_{\ell_p}$ | $C_{\ell_\delta}$[b] | $C_{x_0}$ | PE $x$, mm | PE $y, z$, mm | PE $\theta, \psi$, deg | PE $\phi$, deg |
|---|---|---|---|---|---|---|---|---|
| 62 | 82.7 | 12.5 | 3.35 | 0.750 | 1.8 | 2.1 | 0.15 | 6.7 |
| 65 | 76.0 | 10.3 | 1.84 | 0.737 | 2.1 | 2.0 | 0.11 | 3.5 |
| 67 | 91.8 | 13.9 | 2.30 | 0.744 | 4.9 | 2.3 | 0.16 | 4.0 |
| 66 | 98.8 | 14.5 | 3.11 | 0.745 | 1.2 | 1.9 | 0.20 | 3.6 |
| 54 | 85.8 | 11.2 | 2.20 | 0.648 | 4.5 | 1.6 | 0.12 | 4.6 |
| 44 | 81.6 | 10.0[a] | — | 0.636 | 4.2 | 2.4 | 0.18 | 17.1 |
| 57 | 88.6 | 8.9 | 1.44 | 0.638 | 1.2 | 2.1 | 0.14 | 11.3 |
| 47 | 72.2 | 10.5 | — | 0.610 | 1.7 | 2.1 | 0.19 | 5.7 |
| 60 | 76.3 | — | — | 0.607 | 1.8 | 1.9 | 0.10 | 4.4 |
| 52 | 77.9 | 10.3 | 0.87 | 0.548 | 2.1 | 1.9 | 0.15 | 11.3 |
| 45 | 74.0 | 10.0[a] | — | 0.469 | 1.1 | 1.9 | 0.14 | 7.3 |
| 80 | 72.3 | 12.3 | 1.51 | 0.529 | 1.9 | 1.9 | 0.13 | 4.8 |
| 46 | 71.1 | 10.9 | 1.22 | 0.529 | 2.5 | 2.4 | 0.19 | 5.8 |
| 81 | 74.5 | 10.9 | 0.95 | 0.527 | 2.2 | 2.1 | 0.12 | 6.6 |
| 48 | 73.3 | 10.0[a] | — | 0.487 | 0.9 | 1.3 | 0.31 | 10.2 |
| 82 | 68.8 | 12.6 | 0.69 | 0.477 | 3.7 | 2.2 | 0.16 | 5.6 |
| 74 | 62.4 | — | — | 0.413 | 6.0 | 2.1 | 0.43 | — |
| 72 | 63.7 | 20.0 | — | 0.409 | 7.7 | 2.1 | 0.34 | 5.2 |
| 75 | 61.2 | — | — | 0.425 | 7.4 | 1.9 | 0.52 | — |
| 73 | 62.1 | — | — | 0.398 | 2.9 | 2.1 | 0.22 | — |
| 77 | 49.0 | — | — | 0.390 | 8.0 | 2.8 | 0.43 | — |
| 78 | 55.0 | — | — | 0.354 | 4.4 | 4.8 | 0.53 | — |

[a]Held constant. [b]Due to fin tab angle only.

**Table 4 Aerodynamic results (multiple fits)**

| Shot no. | Mach no. | α max, deg | $C_x$ | $C_{m_\alpha}$ | $C_{n_{p\alpha}}$ | $C_{m_q}$ | $C_{m_{\alpha p}}$ | $C_{\ell_p}$ | PE $x$, mm | PE $\theta, \psi$, deg | PE $\phi$, deg |
|---|---|---|---|---|---|---|---|---|---|---|---|
| 62, 65, 66, 67 | 1.650 | 1.4 | 0.714 (0.009) | −60.0 (0.6) | 274.4 (26) | −1208.5 (370) | −2337.5 (44) | −13.2 (0.09) | 3.4 | 0.14 | 26.7 |
| 66, 67 | 1.689 | 1.4 | 0.745 (0.001) | −62.3 (1.4) | — | 1156.4 (173) | −2155.5 (92) | −14.3 (0.3) | 3.6 | 0.14 | 7.0 |
| 60, 47, 54 44, 57 | 2.137 | 3.3 | 0.627 (0.0009) | −79.8 (0.4) | 261.5 (29) | −2135.0 (270) | −912.2 (45) | −9.8 (0.1) | 3.4 | 0.21 | 14.4 |
| 47, 60 | 2.197 | 3.0 | 0.609 (0.0009) | −72.5 (0.6) | — | −2497.1 (611) | — | −13.6 (0.9) | 1.8 | 0.17 | 7.3 |
| 45, 46, 52 | 2.814 | 2.3 | 0.532 (0.007) | −73.2 (0.8) | — | −1581.8 (202) | −633.6 (134) | −13.0 (0.07) | 5.9 | 0.27 | 4.9 |
| 74, 73, 75 | 3.638 | 3.4 | 0.392 (0.002) | −61.6 (0.5) | — | −5000.0 (418) | — | — | 3.4 | 0.37 | — |

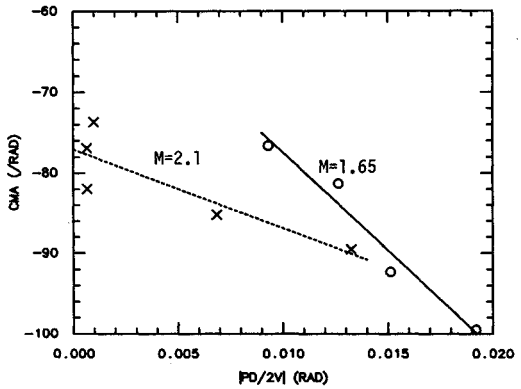


**Fig. 6** $C_{m_\alpha}$ vs $|pd/2V|$ at Mach 1.65 and 2.1.

utilized because the same effect is expected for a negative spin. The solid lines in the figure indicate the best-fit linear correlation lines through the experimental points. It was quite apparent, while conducting multiple fits for the 4 shots at Mach 1.65, that solving for a common $C_{m_\alpha}$ was impossible since the probable errors in yaw and $C_{m_\alpha}$ were quite high. This was alleviated when solving for a unique $C_{m_\alpha}$ for every shot while doing a multiple fit.

Based on Fig. 6, an aspect that was investigated was the aerodynamic term $C_{m_{\alpha p}}$. This is a static pitching moment slope linearly dependent on spin $pd/2V$, or basically an in-plane Magnus moment. This term was chosen as a result of the trends apparent in Fig. 6 and was the obvious one to use. The aerodynamic moment expansion from Ref. 2 was modified to account for this term as follows:

$$M = \bar{q}Ad\left(\bar{C}_{m_\alpha}\frac{w}{V} + \frac{qd}{2V}\bar{C}_{m_q} + \frac{pd}{2V}\bar{C}_{n_{p\alpha}}\frac{v}{V} + \frac{pd}{2V}\bar{C}_{m_{\alpha p}}\frac{w}{V} + \bar{C}_{n_{\gamma\alpha}}\frac{v}{V} + \bar{C}_{m_\delta}\delta_A\cos\phi - \bar{C}_{m_\delta}\delta_B\sin\phi\right)$$

$$N = \bar{q}Ad\left(-\bar{C}_{m_\alpha}\frac{v}{V} + \frac{rd}{2V}\bar{C}_{m_q} + \frac{pd}{2V}\bar{C}_{n_{p\alpha}}\frac{w}{V} - \frac{pd}{2V}\bar{C}_{m_{\alpha p}}\frac{v}{V} + \bar{C}_{n_{\gamma\alpha}}\frac{w}{V} + \bar{C}_{m_\delta}\delta_A\sin\phi + \bar{C}_{m_\delta}\delta_B\cos\phi\right)$$

The 6-DOF multiple-fit results with the term $C_{m_{\alpha p}}$ included on some shot groups are given in Table 4, with the probable error of the coefficients in parentheses.

The first result in Table 4 (shot group 62, 65, 66, 67) gives a $C_{m_{\alpha p}}$ of −2337.5 (45) and a $C_{m_\alpha}$ of −60.0 (0.6), with their respective probable error in parentheses. Without the $C_{m_{\alpha p}}$ term, $C_{m_\alpha}$ was −95 (0.3), and the probable error of the angular motion was 0.33 deg. The probable error of fit was improved by a factor of 2 when $C_{m_{\alpha p}}$ was included. The slope of the best-fit line through the points of Fig. 6 for Mach 1.65 is −2444, which agrees with the value obtained for $C_{m_{\alpha p}}$. Because the probable error of fit was not improved when $C_{m_q}$ and $C_{n_{p\alpha}}$ were introduced in the fitting process, these were not well determined. The high probable error in roll for this shot group was expected because a common $C_{\ell_p}$ was determined, whereas the single fits showed a wide spread in $C_{\ell_p}$ at this Mach number but with good probable error of fits.

**Table 5 Fitting history for multiple shot 66, 67**

| Fit no. | $C_{m_\alpha}$ | $C_{m_q}$ | $C_{n_{p\alpha}}$ | $C_{m_{\alpha p}}$ | PE $\theta, \psi$ deg |
|---|---|---|---|---|---|
| 1 | −93 (0.5) | −426 (461) | — | — | 0.25 |
| 2 | −62 (1.4) | 1156 (173) | — | −2155 (92) | 0.14 |
| 3 | −60 (1.6) | −8041 (1434) | 808 (103) | −2309 (99) | 0.16 |

Shots 66 and 67, which have the highest steady spin rates, also give similar results. Table 5 traces the fitting process for the multiple-fit case, with the associated probable errors at each stage. The probable error of fit improved by a factor of 2 when $C_{m_{\alpha p}}$ was solved, and it deteriorated when $C_{n_{p\alpha}}$ was included. When a coefficient has an effect on the motion, it should improve the fit but, if it has a negligible effect, it should not deteriorate the fit, as shown in the table. This is probably due to solving for similar terms in the matrix of partial derivatives. Solving for all of the coefficients except $C_{m_{\alpha p}}$ gave a probable error of fit of 0.2 deg. This case gives results for $C_{m_\alpha}$ and $C_{m_{\alpha p}}$ that are similar to the previous one.

All of the shots at Mach 2.1 were analyzed with the multiple-fit option. These include some flights at the low spin rates that were lacking at Mach 1.65. Again, the best fit occurred when $C_{m_{\alpha p}}$ was fit, and it was also well determined. The slope of the best-fit line in Fig. 6 for this shot group is −982. The reduced common $C_{m_\alpha}$ agrees well with the shots at slow spin rates (Fig. 6).

The multiple-fit option was again utilized on shots (45, 46, 52) with respective nominal tab angles of 0, 2, and 4 deg at Mach 2.8. This time $C_{m_{\alpha p}}$ was not well determined (PE 135), and the probable error of fit did not improve appreciably (3%). This was expected because there was not much scatter in $C_{m_\alpha}$ at this Mach number (Fig. 5b).

If there is such a dominant effect of spin on $C_{m_\alpha}$, as seen in the multiple-fit reductions, the single fits should improve with the inclusion of $C_{m_{\alpha p}}$ if there is enough variation in the spin

rate. The spin rate as a function of distance for shot 66 is shown in Fig. 7 and varies from 850 rad/s to a maximum of 3500 rad/s. The coefficients at each stage of reduction for shot 66 are given in Table 6, with $C_{m_{\alpha p}}$ included. Case 1 is the result quoted in Table 3. Reducing for only $C_{m_\alpha}$ and $C_{m_q}$ gives a very poor result. The probable error of fit is improved by a factor of 3 when $C_{m_{\alpha p}}$ is included and is not improved by the inclusion of $C_{n_{p\alpha}}$. The results obtained for $C_{m_\alpha}$ and $C_{m_{\alpha p}}$ agree very well with the multiple-fit results, which indicates that there is a strong spin effect on the pitching moment coefficient slope at this Mach number.

Although there were less data for the short-fin models (results not shown here), the multiple fits were also improved at Mach 2 with the inclusion of $C_{m_{\alpha p}}$. There was no noticeable difference in the axial force coefficient between the short- and long-fin model. The roll damping for the short-fin model is less than for the long-fin, as expected. The short-fin model is less stable statically than the long-fin model at Mach 2.5 and higher.

The roll damping term ($C_{\ell_p}$) is linear when plotted against $pd/2V$ at Mach 1.65 (Fig. 8), which indicates a nonlinear variation of the rolling moment with spin.

**Table 6 Fitting history for shot 66**

| Fit no. | $C_{m_\alpha}$ | $C_{m_q}$ | $C_{n_{p\alpha}}$ | $C_{m_{\alpha p}}$ | PE$\theta$, $\psi$, deg |
|---|---|---|---|---|---|
| | | Case 1 (case in Table 3) | | | |
| — | −98.8 | −22564 | 1775 | — | 0.21 |
| | (0.6) | (1775) | (250) | | |
| | | Case 2 | | | |
| 1 | −83 | −8148 | — | — | 0.35 |
| | (9) | (8241) | | | |
| 2 | −68.1 | 397.6 | — | −1858 | 0.13 |
| | (2.7) | (220) | | (160) | |
| 3 | −61.5 | −14457 | 1095 | −2217 | 0.15 |
| | (3.1) | (2828) | (198) | (190) | |

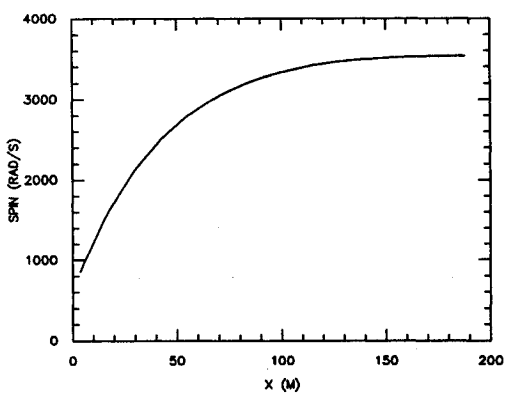


**Fig. 7 Spin vs distance for shot 66.**

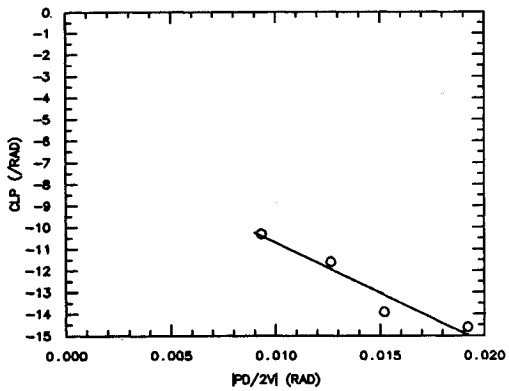


**Fig. 8 Roll damping coefficient vs $|pd/2V|$ at Mach 1.65.**

## Conclusions

It has been demonstrated from free-flight testing of a high $\ell/d$ finned projectile configuration that some aerodynamic coefficients are affected by highly varying spin rates at a given Mach number. This effect was most noticeable in the low supersonic region (Mach 1.5–2.5), decreased as the Mach number increased, and was absent at the very high Mach numbers. The aerodynamic term $C_{m_{\alpha p}}$ explains this variation. It is believed to be the first time that an in-plane Magnus-type effect has been shown to exist, and this could have very important ramifications to designers of finned missiles experiencing high spin rates. Although high spin rates were achieved during these tests, no Magnus moment was apparent.

## Acknowledgments

A joint program of this size involves various people from different establishments. At DREV, thanks are due to Mr. M. Normand, who designed the sabot, and to Mr. J. Evans, who attended the firings at Eglin Air Force Base. Special thanks are due to Mr. B. Cheers of DREV and Mr. G. Winchenbach of Eglin Air Force Base for their many comments, discussions, and suggestions during the data reduction process. Thanks are also due to Mr. R. Whyte, Mr. W. Hathaway, and Mr. B. Wong of General Electric for the computer program modifications that were necessary to handle the high spin rates and the inclusion of the extra aerodynamic term. Finally, I would like to thank Lt. R. Gates, the coordinator, who was most helpful in all stages of the program.

## References

[1]Winchenbach, G.L., Galanos, D.G., Kleist, J.S., and Lucas, B.F., "Description of Capabilities of the Aeroballistic Research Facility," Air Force Armament Lab. TR-78-14, April 1978.

[2]Hathaway, W.H. and Whyte, R., "Aeroballistic Research Facility Free-Flight Data Analysis Using the Maximum Likelihood Method," AFATL-TR-79-98, Dec. 1979.

[3]Watt, R.M., "Free Flight Range Tests of Flechette-Type Projectiles at Nominal Mach Numbers of 4 and 5,"Arnold Engineering Development Center TR-67-259, Jan. 1968.

[4]Rottenberg, M. and Settler, C., "Development of 20 mm Armor-Piercing Cartridge Type MLU-36/C," AFATL-TR-67-94, Aug. 1967.